# Mechanisms by Which Organic Solvent Exchange Transforms Responsive Pure Protein Hydrogels into Responsive Organogels

Natasha Lynn Smith,[iD] Andrew Eagle Coukouma, Ryan S. Jakubek,[iD] and Sanford A. Asher*[iD]

Department of Chemistry, University of Pittsburgh, Pittsburgh, Pennsylvania 15260, United States

Ⓢ *Supporting Information*

ABSTRACT: Responsive pure protein organogel sensors and catalysts are fabricated by replacing the aqueous mobile phase of protein hydrogels with pure ethylene glycol (EG). Exchanging water for EG causes irreversible volume phase transitions (VPT) in bovine serum albumin (BSA) polymers; however, BSA hydrogel and organogel sensors show similar volume responses to protein–ligand binding. This work elucidates the mechanisms involved in this enabling irreversible VPT by examining the protein secondary structure, hydration, and protein polymer morphology. Organogel proteins retain their native activity because their secondary structure and hydration shell are relatively unperturbed by the EG exchange. Conversely, the decreasing solvent quality initiates polymer phase separation to minimize the BSA polymer surface area exposed to EG, thus

decreasing distances between BSA polymer strands. These protein polymer morphology changes promote interprotein interactions between BSA polymer strands, which increase the effective polymer cross-link density and prevent organogel swelling as the mobile phase is exchanged back to water.
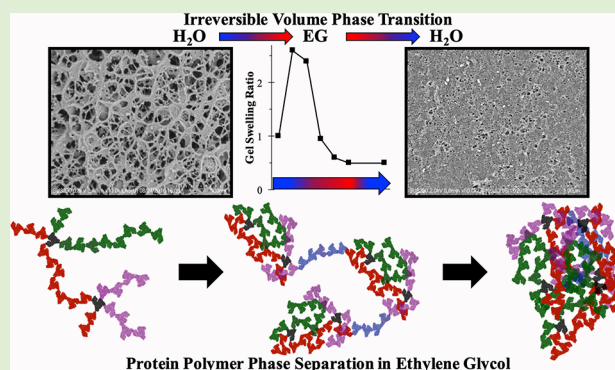
INTRODUCTION

Hydrogels and organogels are versatile materials with numerous applications as sensors,[1–5] catalysts,[6,7] drug delivery materials,[8,9] tissue engineering scaffolds,[10] wound dressings,[11] membranes,[12] and mechanical actuators.[13] These responsive materials consist of two primary components: a stationary phase made up of a 3-dimensional chemically or physically cross-linked polymer network and a liquid mobile phase that facilitates diffusion and mass transport within the polymer network. Hydrogels contain an aqueous mobile phase, whereas organogels contain an organic solvent mobile phase.

Our group pioneered the development of photonic crystal-based colorimetric chemical sensors[14,15] that utilize the hydrogel volume phase transition (VPT) responses to external stimuli such as pH, light, and chemical analytes.[4,16–19] Hydrogels or organogels that have molecular recognition groups attached to the polymer network selectively undergo VPT in response to a specific analyte.[17,18,20,21] This analyte induced VPT shifts the embedded photonic crystal particle spacing, thus shifting the photonic crystal light diffraction.[14–16]

These VPT involve distinct changes in the hydrogel/organogel volume in response to small changes in the hydrogel/organogel chemical environment.[22] These volume changes are caused by osmotic pressures, Π, which derive from changes in the Gibbs free energy, ΔG_{total}.[23,24] Osmotic pressures in the system induce mass transfer of the mobile phase: either partitioning the mobile phase into the polymer network to cause swelling, or expelling the mobile phase to cause shrinking. When the polymer and mobile phase are at equilibrium, $\Pi_{total} = \partial \Delta G_{total}/\partial V = 0$. In general, for hydrogel/organogel chemical sensors, analyte recognition must induce a change in the Gibbs free energy to actuate a VPT.

Recently, we developed several stimuli responsive pure protein hydrogels that sense pH, glucose, yeast cells, drugs, surfactants, and fatty acids.[3,5,25] These protein hydrogels have selective chemical responses because the constituent proteins show specific molecular recognition. There exists a large body of research developing functional pure protein hydrogels using a variety of fabrication methods, such as glutaraldehyde cross-linking, or enzyme catalyzed cross-linking of proteins, and self-assembly of engineered proteins.[6,7,9,26–28]

There are very few studies of pure protein organogels,[29,30] despite the intense interests in utilizing protein chemistries in organic solvents for industrial applications such as enzymatic synthesis of pharmaceuticals and biofuels,[31,32] as well as for sensing and degrading toxic compounds important to the defense industry.[33,34] Organic solvents typically denature proteins and significantly decrease protein reactivity.[35] This has led to the development of several techniques to stabilize proteins against denaturation or deactivation by organic solvents.[36–38]

We very recently developed methods to fabricate stimuli responsive pure protein organogels for sensing and catalysis applications.[39] The pure protein organogels are fabricated from pure protein hydrogels by using a stepwise solvent exchange that replaces the aqueous mobile phase of pure protein hydrogels with ethylene glycol (EG). Chemically cross-linked pure protein polymer hydrogels are fabricated by polymerizing protein monomers in solution using glutaraldehyde. The proteins are immobilized by this protein polymerization such that the proteins retain their native reactivity after the aqueous mobile phase is replaced with pure EG. Protein immobilization is a widely used strategy to stabilize proteins against denaturation, which typically enhances protein activity in organic solvents.[36,37,40−44]

We believe that our photonic crystal BSA organogel sensor[39] is the first reported responsive pure protein organogel to exhibit a VPT in response to ligand binding. The polymerized BSA in the organogels bind the same ligands as do the BSA hydrogels[3] and the native protein monomers.[45,46] The BSA hydrogels and organogels also exhibit similar VPT responses to ligand binding, swelling when BSA binds charged ligands like ibuprofen and fatty acids.

Recent publications have investigated conformational changes[98] and phase transitions[99] in dipeptide organogels. For example, Yuan et al.[99] demonstrated that self-assembled diphenylalanine organogels are responsive to changes in the solvent composition. The addition of chloroform to the hexafluoropropanol/toluene mobile phase caused organogel swelling, whereas the addition of water caused a gel to crystal transition. The development of more selective responsive hydrogel and organogel materials is enabled by utilizing proteins instead of simple dipeptide molecules because proteins have evolved to have specific ligand binding pockets. However, the responsive protein polymers reported on here and in our previous publication[39] have substantially more complex polymer−mobile phase interactions compared to the homogeneous dipeptide organogels, due to their heterogeneous composition of 20 possible amino acids, leading to interesting VPT phenomenon in response to environmental changes.

The water to EG solvent exchange that transforms responsive BSA hydrogels into responsive BSA organogels induces a large VPT that decreases the organogel volume as the concentration of EG in the mobile phase increases. As shown herein, this solvent exchange induced VPT is irreversible; rehydrating the BSA organogel by exchanging the EG mobile phase back to water does not result in reswelling.

This VPT irreversibility is enabling for developing our selective protein organogel sensors because it creates chemical sensors that are insensitive to fluctuations in humidity and water concentration, thus increasing their potential applications. EG was utilized as the mobile phase due to its low vapor pressure. Protein organogels that utilize an EG mobile phase are more resistant to evaporation compared to protein hydrogels, increasing the time scales these responsive materials can function when exposed to ambient conditions. Thus, these responsive protein organogels with low vapor pressure mobile phases could be utilized for sensing gas phase analytes. EG is hydroscopic, therefore, the organogel's insensitivity to the EG water content is highly advantageous for developing gas sensing materials as it eliminates false negatives and positives that may result from changes in humidity.

In this work, we characterize the protein secondary structure, protein hydration, and the protein polymer morphology in the BSA hydrogels, organogels, and water incubated organogels in order to elucidate the mechanisms involved in this irreversible VPT. The BSA secondary structure in the hydrogel, organogel, and water incubated organogel is determined using the UVRR AmIII$_3$ band frequencies that are sensitive to changes in the peptide secondary structure.[47] The protein solvation shell water layer in the BSA organogel is estimated using the strong NIR absorbance of water. Cryo-SEM is used to image the morphology of the BSA hydrogels and water incubated organogels, elucidating the super-molecular structure of the protein polymer networks. The change in the protein polymer surface area exposed to the mobile phase is determined by titrating the BSA amino acid carboxyl groups.

We discuss the chemistry and mechanisms involved in the BSA hydrogel to organogel transformation that result in this large irreversible VPT shrinking. VPT that dramatically decrease the volume of cross-linked polymer networks are often driven by polymer phase separations; for example, the extraordinarily large VPT of p(isopropylacrylamide) hydrogels is caused by lower critical solution temperature phase separation, which is initiated by a hydrophobic collapse of the isopropyl groups from water.[48,49] We posit that the origin of the irreversible VPT stems from interprotein interactions formed during the BSA polymer phase separation. These interprotein interactions act as additional polymer network cross-links that prevent BSA polymer swelling of the water incubated organogel.

■ EXPERIMENTAL SECTION

Materials. BSA (>98%; lyophilized powder, essentially fatty acid free) and Sigmacote were purchased from Sigma-Aldrich and used as received. Glutaraldehyde (50 wt %) in water was purchased from Sigma-Aldrich and diluted to 12.5 wt % glutaraldehyde with nanopure water. Ethylene glycol (certified, <0.2% water) was purchased from Fisher Chemical and used as received. Nanopure water was produced using a Barnstead NANOpure infinity system. Type A brass planchets were purchased from Ted Pella.

Fabrication of BSA Hydrogels, Organogels, and Organogels Incubated in Water. BSA hydrogels were fabricated by polymerizing BSA monomers in solution using glutaraldehyde to form covalent linkages between BSA lysine residues, as described in our previous publications.[3] Glass microscope slides were treated with Sigmacote to make their surfaces hydrophobic. A ∼410 μm thick spacer was created by adhering layers of 3 M Scotch Magic Greener tape along the edges of the slide. The spacer ensures that the polymerized hydrogel film has a uniform thickness.

A 200 mg/mL BSA stock solution was prepared by dissolving lyophilized BSA powder in nanopure water. BSA hydrogel polymerization was initiated by adding 64 μL of a 12.5 wt % glutaraldehyde solution to 1.0 mL of the BSA stock solution. The solution was shaken to mix the components, and then poured onto the glass slide within the spacer. A second glass slide was placed on top and pressed firmly into the spacer to expel excess solution. The BSA/glutaraldehyde solution was polymerized for 3 h at room temperature. After polymerization, the slides were separated, releasing the BSA hydrogel films. BSA hydrogels were washed with large amounts of nanopure water for 2 days to remove unreacted BSA and glutaraldehyde.

BSA organogels were fabricated by using a stepwise solvent exchange process that replaces the aqueous mobile phase with EG.[39] BSA hydrogels were incubated in aqueous solutions containing increasing concentrations of EG for 24 h each during which the solvent was replaced 3 times with ∼250 mL of fresh solution. The samples were placed on a shaker to mix the BSA gels and solution

during the exchange. The BSA hydrogels were transferred from nanopure water to 30% (v/v) EG in water, then to 50% (v/v) EG in water, and then to 70% (v/v) EG in water. Finally, the BSA gels were equilibrated with pure EG for 2 days to complete the solvent exchange. The ~250 mL volume of pure EG was replaced 6 times over those 2 days to ensure that excess water was removed from the mobile phase.

Water incubated BSA organogels were fabricated by exchanging the pure EG mobile phase of BSA organogels back to pure water. The stepwise solvent exchange described above was reversed; BSA organogels were incubated for 24 h on the shaker in 70% (v/v) EG, followed by 50% (v/v) EG, and then 30% (v/v) EG. The ~250 mL volume of solvent was replaced 3 times each day. Finally, the organogels were incubated in nanopure water for 3 days where ~250 mL of fresh water was replaced 4 times daily to ensure that all the EG was removed from the mobile phase.

Volume Phase Transition Measurements. Directly after polymerization of the BSA hydrogels, before washing the hydrogels in water, the hydrogel films were cut into smaller square pieces using a razor blade. The dimensions of each piece were measured using a digital micrometer. The precisely measured hydrogel samples were washed in nanopure water followed by the stepwise solvent exchange steps described above. The dimensions of the hydrogel/organogel samples were measured after incubation in each solvent composition.

The BSA hydrogel pieces exist as free-floating films that appear to swell isotropically. Therefore, the hydrogel and organogel volumes can be calculated from the measured gel areas using the swelling ratio $\left(\frac{A}{A_i}\right)^{3/2} = \frac{V}{V_i}$, where A_i and V_i are the initial area and volume of the BSA hydrogel piece directly after polymerization, while A and V are the area and volume of the BSA hydrogel or organogel after incubating in a particular EG/water solution.

The initial BSA concentration in the hydrogel directly after polymerization is 200 mg/mL. This concentration corresponds to an initial BSA polymer volume fraction of $\phi_i = 15\%$, given the specific volume of BSA in water is 0.734 cm³/g.[50] The BSA polymer volume fraction in the hydrogel or organogel after swelling or shrinking in solvent is calculated using the volume swelling ratio (eq 1).

$$\phi = \phi_i \times \frac{V}{V_i} \tag{1}$$

UV Resonance Raman Spectroscopy of BSA Hydrogels and Organogels. UV Resonance Raman (UVRR) spectroscopy was used to investigate the secondary structure of BSA monomers free in solution and polymerized BSA in the hydrogel, organogel, and water incubated organogel.

The instrumentation used was previously described in detail by Bykov et al.[51] We generated ~204 nm excitation light by first frequency tripling the fundamental of a Nd:YAG laser to ~355 nm. The ~355 nm light was then Raman shifted to ~204 nm using the fifth anti-Stokes harmonic of hydrogen gas (30 psi). The 204 nm light was focused onto a spinning Suprasil quartz NMR tube containing the sample, and a ~165° backscattering geometry was used to collect the scattered light. The scattered light was dispersed using a home-built double spectrometer in a subtractive configuration. The dispersed light was imaged using a liquid nitrogen cooled back-thinned CCD camera (Princeton Instruments) with a Lumogen E coating.

NIR Absorption Measurements of BSA Organogel Water Content. The strong water absorption band at 1915 nm was used to calculate the water content in BSA organogels using a protocol similar to that of our previous publication.[16] The NIR absorption between 1400 and 2000 nm was measured for solutions containing 1.6 mL of EG and 0, 5, 10, 15, 20, and 25 μL water in a 5 mm path length quartz cuvette.

The absorption of 1 and 2 layers of the BSA organogel film was also measured. The 420 μm thick organogel film was cut to the size of the cuvette inner wall (~1 cm × 4 cm). Excess EG on the surface of the organogel films was removed by blotting the films with filter paper until the surface appeared dry. The film was then placed on the wall of the quartz cuvette. Experimental details of these measurements are provided in the Supporting Information. The Supporting Information also includes the NIR absorbance of the EG/water solutions and the BSA organogels, the calibration curve for water absorption in EG at 1915 nm, and discusses the calculation of the water concentration in the organogel.

Cryo-SEM of BSA Hydrogels and Water Incubated BSA Organogels. *Preparation of BSA Solution, BSA Hydrogel, and Water Incubated BSA Organogel Samples for Cryo-SEM.* Cryo-SEM imaging was performed at the University of Minnesota College of Science and Engineering Characterization Facility in collaboration with Chris Fretham and Hanseung Lee.

BSA was dissolved in nanopure water to make 200 mg/mL BSA solutions. The BSA solution samples were prepared for Cryo-SEM by sandwiching a 3 μL aliquot of this BSA solution between two brass planchets. The Ted Pella Type A planchets were 3 mm in diameter. They contained a 2 mm diameter, 100 μm deep well in the center. The cylindrical cavity between the planchets that contained the samples was 200 μm thick.

The BSA hydrogel samples were prepared by polymerizing the BSA/glutaraldehyde solution between two Type A brass planchets, in the 2 mm diameter, 200 μm thick cavity. The surface of the brass planchets was abraded prior to hydrogel polymerization to promote adhesion between the hydrogel and planchet so that the hydrogels fractured after freezing.

Cryo-SEM imaging requires sublimation of the water mobile phase to reveal the polymer stationary phase. Protocols to flash freeze pure EG and subsequently sublimate the EG mobile phase do not currently exist. Therefore, the EG mobile phase was exchanged back to water to form the water incubated organogel as described above. The thickness of the water incubated organogel film was between 0.18 and 0.2 μm after the solvent exchange process was completed. A specialized die was fabricated by the University of Pittsburgh machine shop and used to cut 1.8 mm diameter discs from the BSA organogel films. These organogel discs fit snuggly into the 2 mm diameter/0.2 mm thick cavity between the two Type A brass planchets.

High pressure flash freezing of the samples between brass planchets was done using a BAL-TEC HPM 010 high pressure freezing machine at 2100 bar with liquid nitrogen (LN₂). High pressure freezing promotes formation of vitreous ice and prevents the formation of ice crystals that can destroy the delicate network structure.[52] Samples were stored under constant cryogenic temperatures.

The planchets containing frozen samples were affixed to the sample holder while still immersed in a LN₂ bath. A photograph of the sample holder is shown in Figure S1 of the Supporting Information. The sample holder was then transferred to the Leica EM ACE600 high vacuum sputter coater using the Leica VCT100 shuttle. The Leica VCT100 shuttle and the Leica EM ACE600 instrument were cooled with LN₂ prior to transferring the samples. It is important that the sample remains at cryogenic temperatures to avoid ice crystal formation. The pressure and temperature inside the chambers were maintained at 1.5×10^{-5} mbar and at −166 °C. A cold knife was used to remove the top planchet, fracturing the sample to reveal the inner hydrogel and organogel polymer networks.

Vitrified ice in the interstitial spaces of the protein polymer network was removed by sublimation, a process sometimes referred to as Cryo-etching.[52] The temperature inside the chamber was increased from −166 to −100 °C at a rate of 3 °C/min. The pressure was kept at 1.5×10^{-5} mbar. The sample was held at −100 °C for 40 min to allow significant sublimation of vitreous ice at the surface. This reveals the protein polymer network. A cold trap kept at −160 °C was placed over the sample to prevent sublimated water vapor from condensing back onto the sample.

After 40 min, the temperature was decreased to −115 °C, halting the sublimation of water. After sublimation, samples were sputter coated, depositing a 2.5 ± 0.03 nm layer of platinum on the sample. The thickness of the Pt coating was determined by the frequency shift of a quartz crystal oscillator, calibrated for the density of the Pt deposited.
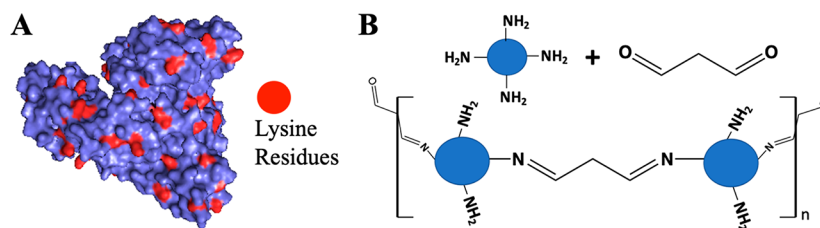
Figure 1. (A) BSA protein structure showing lysine residues highlighted in red. Structure obtained from RCSB Protein Data Bank, 3V03. Image made using PyMol software. (B) One of the possible glutaraldehyde interprotein cross-linking reactions; the aldehyde and lysine amine group form a Schiff base that covalently links the two proteins.

Cryo-SEM of Frozen Hydrated BSA Hydrogels and Water Incubated Organogels. The samples were transferred to the Hitachi SU8230 field emission gun scanning electron microscope under vacuum at cryogenic temperatures in the Leica VCT100 shuttle. The Leica VCT100 Cryo-stage temperature was maintained at −115 °C throughout imaging. Samples were examined using low accelerating voltages (0.8–2 kV) to avoid charging and subsequent damage to the sample. Samples were left in the SEM chamber overnight under vacuum after Cryo-SEM imaging was complete. As the temperature inside the vacuum chamber slowly increased throughout the night, the samples became freeze-dried. The freeze-dried samples were imaged the next day before the SEM was cooled with LN$_2$. The stage temperature was ∼10 °C during SEM imaging of the freeze-dried samples.

We used the NIH software ImageJ[53] to analyze the BSA polymer networks in the Cryo-SEM micrographs. The BSA polymer strand diameters, pore diameters, and the length of the protein polymer strands were measured in several Cryo-SEM images and averaged.

Titration of BSA Hydrogels and Water Incubated Organogels. BSA hydrogels were prepared as described above and cut to various sizes directly after polymerization before incubating in water. The concentrations of BSA in these BSA hydrogels are 200 mg/mL. The area of each freshly prepared 420 μm thick BSA hydrogel piece was measured and the moles of protein contained in each BSA hydrogel piece was calculated from its volume. The hydrogel samples were then equilibrated in nanopure water.

Half of the BSA hydrogel samples were transformed to BSA organogels using the stepwise EG exchange process. These organogel samples were then rehydrated with nanopure water by reversing the stepwise solvent exchange process. These samples were then incubated in water for 3 days, during which the water was replaced twice daily with fresh nanopure water.

The BSA hydrogels and water incubated organogels were placed in 2 mL of pH 7.5 nanopure water. The pH was monitored using a Hanna Instruments HI5522 pH meter with a Hanna Instruments HI 1083 microelectrode as 5–20 μL aliquots of 0.1 M HCl titrant were added to the solutions containing the gels. After each addition of HCL, the solution was mixed for 15 min before the pH was recorded. The pH was then plotted against $\frac{\text{mol HCl added}}{\text{mol BSA}}$. Six replicate measurements were performed for both the BSA hydrogels and water incubated organogels.

■ RESULTS AND DISCUSSION

Responsive pure protein hydrogels are fabricated by polymerizing BSA protein monomers using glutaraldehyde to form covalent linkages between BSA lysine residues (Figure 1). Glutaraldehyde is a commonly used protein cross-linker and fixative that has little impact on the native protein structure and the native protein reactivity.[41,54] We use the term "*interprotein* cross-links" to specifically describe the short glutaraldehyde linkages between BSA proteins in the pure protein polymer chains. This is distinct from the *polymer* cross-links that define points where the protein polymer chains

interconnect to form the 3-dimensional hydrogel polymer network.

Glutaraldehyde is most reactive toward lysine residues on the protein surface.[54] BSA contains 60 lysine residues, 34 of which are located on the BSA surface (Figure 1A) and are available for glutaraldehyde interprotein cross-linking.[55] The BSA surface lysine residues are up to 20–24 Å apart.[55] Glutaraldehyde reacts in aqueous solutions to form a mixture of glutaraldehyde monomers and glutaraldehyde polymers of various lengths.[54] Thus, both interprotein and intraprotein cross-linking can occur.

Intraprotein cross-linking is favored at low protein and glutaraldehyde concentrations.[54] At high protein concentrations and at higher glutaraldehyde/protein ratios (typically >25), interprotein cross-linking is favored.[54] The 27 glutaraldehyde/BSA ratio that was used to polymerize the 200 mg/mL BSA solution should favor interprotein cross-linking over intraprotein cross-linking, forming a polymer of covalently linked protein monomers. One possible interprotein cross-linking reaction is shown in Figure 1B, where monomeric glutaraldehyde reacts with two lysine residues to form a Schiff base. The formation of interprotein cross-links is evident from the formation of the insoluble protein polymer network that makes up the hydrogel. These elastic BSA hydrogels are sufficiently robust to be easily handled.

Cryo-SEM Imaging of BSA Hydrogel Morphology and Topology. We utilized Cryo-SEM to image the BSA hydrogel morphology in the hydrated state.[52,56,57] The hydrogel morphology is defined as the supermolecular structure of the 3D polymer network that gives rise to the polymer strand diameters, polymer strand lengths, and the network pore sizes.[58,59] Polymer morphology can significantly impact the hydrogel properties, such as their swelling behavior, which affects hydrogel sensing and drug release behaviors, and their mechanical properties.[12,60] For example, hydrogel networks with increased cross-link density form increasingly more robust materials that exhibit smaller VPT in response to analyte recognition.

Macroscopically, our BSA hydrogels are transparent and appear to be homogeneous films. These BSA hydrogel films also exhibit homogeneous and isotropic VPT swelling in response to hydrogel protein–ligand binding.[3,39] At the nano- and/or microscale, the BSA hydrogel supermolecular structure appears relatively heterogeneous, as shown in Figure 2. The BSA hydrogel network pore sizes have a large distribution of diameters, ranging from ∼50 to ∼200 nm.

The Cryo-SEM micrographs reveal a discernible BSA polymer network once the vitreous ice is sublimed from the sample (Figure 2A–D). The 40 min sublimation time removes most of the bulk water near the sample surface, revealing the protein polymer network morphology of our frozen hydrated
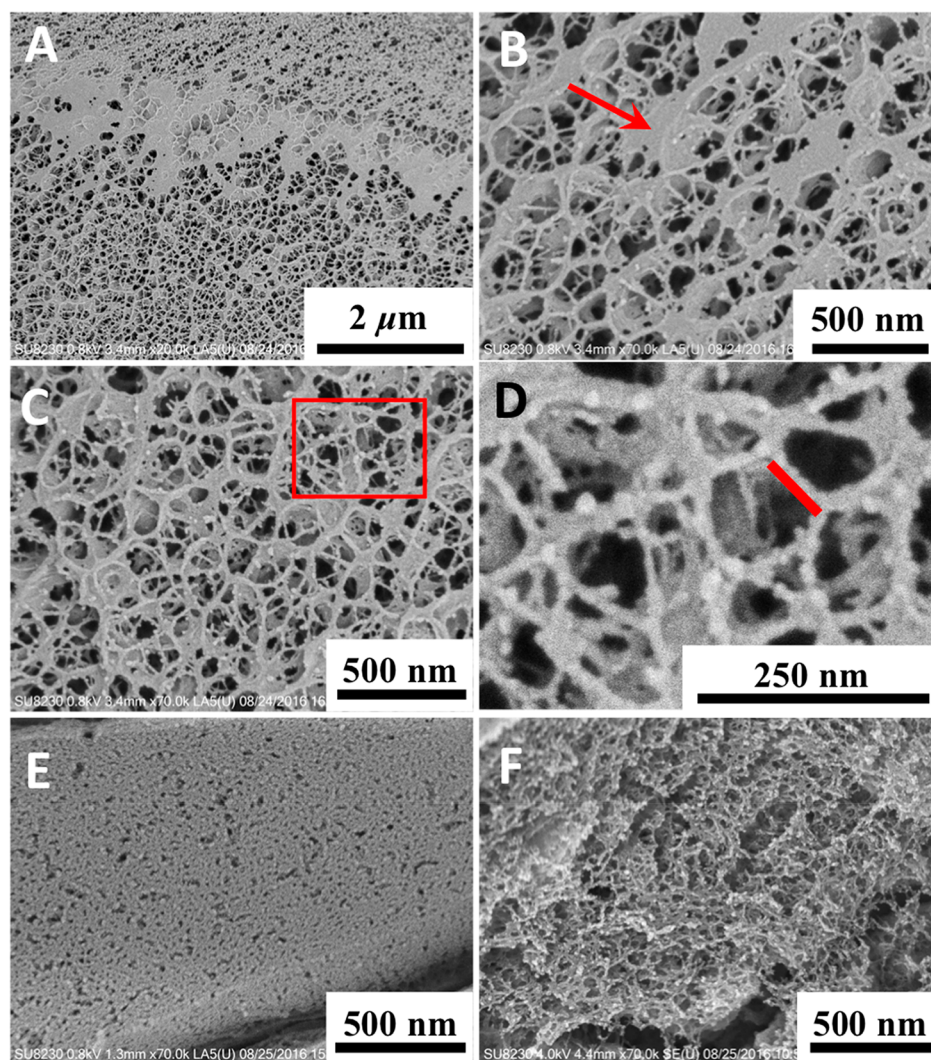
Figure 2. Cryo-SEM of frozen hydrated BSA hydrogels (A−D) and of BSA monomer solutions prior to polymerization (E), and a non-Cryo-SEM of a BSA hydrogel that was freeze-dried (F). Frozen hydrated BSA hydrogels are shown at 20K magnification (A); 70K magnification (B), red arrow points to vitreous ice remaining in the sample; 70K magnification (C), red box indicates the area that is enlarged in Figure 2D. (D) Enlarged area from Figure 2C where the thin BSA polymer strands are clearly visible. The red line highlights one of the measured protein polymer strand lengths. (E) Cryo-SEM of BSA monomer solutions before glutaraldehyde polymerization: 70K magnification. (F) Non-Cryo-SEM of freeze-dried BSA hydrogel: 70K magnification.

BSA hydrogel. Figure 2B shows an area with many patches of vitreous ice remaining on the sample. The red arrow in Figure 2B points to one of these remaining vitreous ice patches. BSA is a hydrophilic water-soluble protein. Thus, solvation shell waters will be difficult to sublimate under these conditions in 40 min and will tend to remain bound to the polymerized BSA.

Shown in Figure 2A−D, the hydrogel consists of a 3D network of interconnected thin BSA polymer strands. The BSA polymer strand diameters were measured in areas where vitreous ice had mostly sublimated, as shown in Figure 2D. The BSA hydrogel is primarily composed of BSA polymer strands having diameters of ~15 ± 5 nm.

These ~15 nm BSA polymer strand diameters are roughly the width of a single hydrated BSA protein monomer. X-ray diffraction measurements of BSA crystals determined that the BSA monomer has dimensions of ~4 × 6.5 × 7.5 nm^3.[61] We expect that the measured dimensions of a single BSA in our samples will be larger than the crystal structure dimensions due to its bound water layers and its Pt coating. Terahertz

spectroscopy has shown that the water solvation shell can extend up to ~0.8−1.5 nm from the protein surface.[62,63] The 2.5 nm Pt sputter coating will also increase the dimensions of the hydrated BSA polymer strands. These measured BSA polymer strand diameters (Figure 2) are roughly similar to the expected dimension of a single, Pt coated, hydrated BSA protein.

From these high resolution Cryo-SEM images of hydrated BSA hydrogels, we can detect the polymerized BSA hydrogel topology,[64] i.e., how the BSA protein monomers are interconnected by the glutaraldehyde interprotein cross-linking to form the polymer network. The ~single BSA diameter of the protein polymer strands indicates that most of the globular proteins are bound together into roughly linear BSA chains, reminiscent of a pearl-necklace-like structure. Polymer cross-links in the BSA hydrogel network are created by a protein that forms ≥3 interprotein cross-links that connect two or more of these BSA polymer strands, as illustrated in Figure 3.
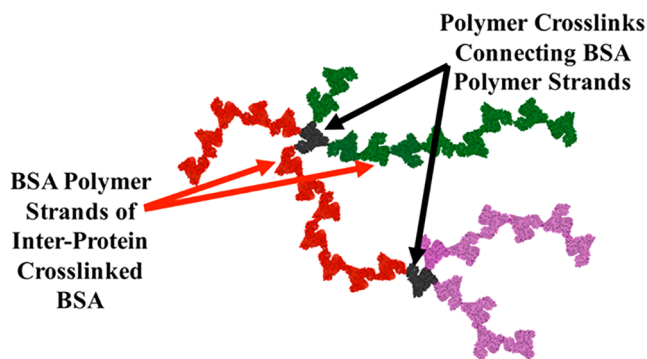
Figure 3. Proposed BSA hydrogel topology based on the Figure 2 Cryo-SEM images. Black arrows point to polymer cross-links, where a BSA forms interprotein cross-links that connect two polymer strands. Red arrows point to the different protein polymer strands that are colored red, green, and pink.

We can approximate the molecular weight between cross-links in the BSA hydrogel network by estimating the number of proteins (MW: 66 463 g/mol BSA) in the polymer strands between polymer cross-links. The red line in Figure 2D highlights a measured polymer strand length. The BSA polymer strand lengths correspond to ~5–30 BSA proteins; i.e., the molecular weight between cross-links in the BSA polymer network is between ~3×10^5 and 2×10^6 g/mol.

The polymer cross-link density is the dominant factor determining the elastic free energy storage of the responsive BSA hydrogel.[23,65] Increasing the polymer cross-link density limits VPT swelling and shrinking. The cross-link density is inversely proportional to the average molecular weight between cross-links.

There are clear differences between the BSA hydrogel morphology (Figure 2A−D) and the morphology of the BSA monomer solution before glutaraldehyde polymerization (Figure 2E). Cryo-SEM images of the BSA monomer solution lack the characteristic interconnected polymer network observed for the BSA hydrogels. This difference between the glutaraldehyde polymerized BSA hydrogel and the BSA monomer solution confirms that predominantly interprotein cross-links are formed by the polymerization of 200 mg/mL BSA solutions at a glutaraldehyde/BSA protein ratio of 27.

Cryo-SEM is uniquely able to probe hydrated samples like hydrogels without significantly altering the protein polymer morphology.[56,57,66] In contrast, non-Cryo/traditional SEM techniques require sample drying prior to SEM imaging. Drying the hydrogel results in the collapse of the polymer network. It is much more difficult to observe and measure the individual polymer strands in non-Cryo-SEM images where BSA hydrogel samples are freeze-dried (Figure 2F). Freeze-dried BSA hydrogel samples also appear to have smaller pores compared to those of the frozen hydrated samples (Figure 2A−D).

EG Solvent Exchange Causes Irreversible VPT. The stepwise solvent exchange from water to EG transforms responsive BSA hydrogels into responsive BSA organogels that sense protein−ligand binding in the pure organic solvent environment.[39] This EG exchange causes a large VPT that decreases the organogel volume. This VPT is irreversible with respect to the mobile phase composition. Attempting to rehydrate the BSA organogel by reversing the stepwise solvent exchange back to water does not cause organogel swelling. The

volume swelling ratios, V/V_0 (red circles), and the resulting BSA polymer volume fractions, φ (black squares), are shown in Figure 4, beginning with the initial BSA hydrogel directly after
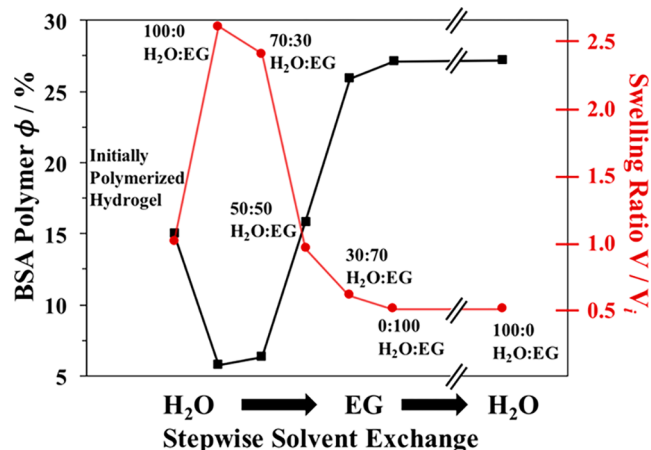

Figure 4. Dependence of the BSA polymer volume fraction, ϕ (left axis, black squares), and the swelling ratio, V/V_i (right axis, red circles), as a function of mobile phase composition during the stepwise water to EG exchange. The breaks in the graph illustrate the stepwise solvent exchange from pure EG back to pure water.

glutaraldehyde polymerization (φ = 15 vol %), and for each subsequent solvent exchange step in the hydrogel to organogel transformation.

The BSA hydrogel initially swells when incubated in water after polymerization until the system comes to equilibrium: $\Pi = \frac{\partial \Delta G_{total}}{\partial V} = 0$. BSA hydrogel swelling in nanopure water decreases the BSA polymer volume fraction from φ = 15 vol % to φ = 6 vol % BSA.

The hydrogel then shrinks as the concentration of EG in the mobile phase increases. The final organogel volume equilibrated in pure EG is roughly half that of the initially fabricated hydrogel. This produces an organogel where the BSA polymer volume fraction is φ = 27 vol %.

Rehydrating the organogel by exchanging the EG mobile phase back to water does not cause organogel swelling. The BSA organogel does not reswell after incubating in water for over 7 days, nor does it swell when the solution is mildly heated to 45 °C. This temperature is below the 57 °C temperature that induces BSA conformational changes.[67] Above 57 °C, swelling may result from protein unfolding. The BSA polymer volume fraction of these water incubated BSA organogels is equal to that of the BSA organogel in EG, φ = 27 vol % BSA.

Flory polymer solution theory is often used to describe the VPT phenomenon,[23] which describes the VPT in terms of osmotic pressures in the system that drive the volume change. These osmotic pressures derive from Gibbs free energy changes in the polymer−mobile phase system. The change in the total Gibbs free energy, ΔG_{total}, has contributions from free energy of mixing changes, ΔG_{mix}, elastic free energy changes, ΔG_{el}, and ionic free energy changes, ΔG_{ion}.[21,68] Changes in the mobile phase composition often induce ΔG_{mix}. Typically, ΔG_{el} and ΔG_{ion} are expected to be small for a simple solvent exchange.

The VPT that results in a dramatic decrease in volume suggests that phase separation of the BSA polymer and mobile

phase occurs during the water to EG exchange. The irreversibility very generally indicates that there is a hysteresis in the total Gibbs free energy between the BSA hydrogel and water incubated BSA organogel. The mechanisms of this phase separation and the origin of this irreversible VPT are discussed below.

BSA Hydrogel, Organogel, and Water Incubated Organogel Secondary Structures. The secondary structures of BSA hydrogels, organogels, and water incubated organogels were investigated using UV Resonance Raman (UVRR) spectroscopy. UVRR spectroscopy is a powerful tool for investigating the hydrogen bonding,[69,70] solvation environment,[71,72] and secondary structure[47,73,74] in proteins.[75,76] UVRR measurements were performed with an excitation wavelength of ~204 nm that is in resonance with the secondary amide $\pi \rightarrow \pi^*$ transitions of the polypeptide backbone.[76] This enhances the Raman scattering of vibrations that couple to the backbone amide electronic transitions.[76]

The UVRR enhanced amide III$_3$ band frequency is highly sensitive to the Ramachandran Ψ torsion angles of the peptide backbone, enabling quantitative analysis of the protein secondary structure.[47,74] The AmIII$_3$ band, found in the ~1200−1300 cm^{-1} spectral region, consists primarily of C−N stretching and NH bending of the peptide bond.[76] The frequency of the AmIII$_3^s$ band sinusoidally depends on the Ramachandran Ψ torsion angle of the peptide bond.[47,74] Mikhonin et al. developed equations to calculate the Ramachandran Ψ angles from the measured AmIII$_3^s$ frequencies.[47]

The distribution of secondary structure populations in proteins gives rise to a particular set of Ψ angles. The secondary structure distribution inhomogeneously broadens the AmIII$_3$ band. The secondary structures in our BSA proteins are determined from the broadened AmIII$_3$ Raman bands. The AmIII$_3$ band shape is fitted to a series of Lorentzians whose sum fits the AmIII$_3$ Raman band shapes. Each Lorentzian band correlates to a particular Ψ angle frequency. The details of the calculated distribution of protein secondary structures in the BSA hydrogels, organogels, and water incubated organogels are provided in the Supporting Information.

We reproduced UVRR measurements of the BSA hydrogel and BSA monomers in aqueous solution. The reproduced UVRR spectra, shown in Figure S2, agree with previous measurements.[3] The AmIII$_3$ band shapes of the polymerized BSA hydrogel and BSA monomer are essentially identical, indicating that the protein secondary structure is not perturbed by the glutaraldehyde interprotein cross-linking that forms the BSA polymer network.

In both the BSA monomer and the BSA hydrogel, the fit of the AmIII$_3$ band shape produces a dominant Lorentzian band at ~1263 cm^{-1}; this AmIII$_3^s$ frequency correlates to a Ψ angle of ~−47°.[47,74] This Ψ angle derives from an α-helical secondary structure. The area under the Lorentzian band at 1263 cm^{-1} accounts for ~65% of the total AmIII$_3$ band intensity, indicating that BSA is predominantly α-helical. Other investigations on native BSA monomers also found the BSA secondary structure to be ~67% α-helical.[77,78]

The BSA organogel AmIII$_3$ band is shifted to a higher frequency from that of the BSA hydrogel (Figure 5). The negative peak in the hydrogel−organogel difference spectrum at ~1265 cm^{-1} (green spectrum in Figure 5) highlights the differences in the two AmIII$_3$ bands. This indicates that the α-helix type AmIII$_3$ band has an increased intensity in the
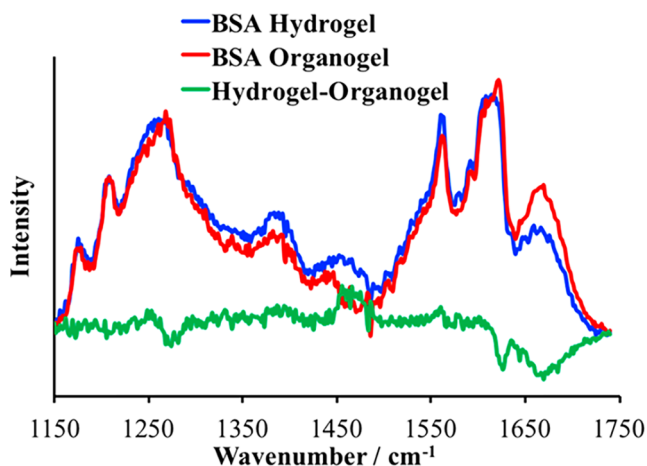

Figure 5. UVRR spectra of BSA hydrogel (blue), BSA organogel (red), and BSA hydrogel−organogel difference spectrum (green). The broad AmIII^3 band at ~1240−1270 cm^{-1} results from the distribution of peptide backbone Ψ angles used to calculate the protein secondary structure. Spectral differences at ~1460 cm^{-1} result from the subtraction of an intense EG Raman peak in the BSA organogel.

organogel compared to the hydrogel. The BSA proteins in the organogel show a ~4% increase in α-helical secondary structures compared to that of the BSA hydrogels.

This result is consistent with previously reported data for immobilized albumins in the presence of EG.[79,80] For example, Wasacz et al. used IR/ATR spectroscopy to investigate the structure of human serum albumin (HSA) that was adsorbed onto a substrate in water, EG, and methanol.[79] They observed an increased intensity of the α-helix AmIII$_3$ band when HSA was exposed to EG. Organic mobile phases generally decrease the solvent's ability to compete for hydrogen bonds compared to water. As a result, the proteins form more intrapeptide hydrogen bonding which increases the propensity for α-helix and β-sheet secondary structure formation.

The UVRR spectra of water incubated BSA organogels reveal that the ~4% increase in the BSA organogel α-helical conformations is reversible when EG is exchanged back to water. The AmIII$_3$ band for the water incubated organogel is essentially identical to that of the BSA hydrogel (Figure 6), indicating that the BSA hydrogel and water incubated organogel have similar secondary structures.

The EG appears to be completely washed out of the organogel during the EG to water exchange. The intense EG Raman peak at ~1460 cm^{-1} in the UVRR BSA organogel spectrum does not appear in the water incubated BSA organogel spectrum.

We also examined the frequency of the AmI band of the BSA hydrogel, BSA organogel, and rehydrated BSA organogel. The AmI band in the ~1650−1700 cm^{-1} spectral region consists predominantly of the C═O stretching motion of the peptide backbone.[76] The BSA hydrogel, BSA organogel, and water incubated BSA organogel all have AmI bands at about 1665 cm^{-1}. The constant AmI band frequency in the BSA hydrogel and organogel spectra indicates that the hydrogen bonding and dielectric environments of the protein backbone amides are similar for the polymerized BSA proteins in the water and EG mobile phases.[69,70,75] This is unexpected since the dielectric constant of EG is significantly lower than that of water. This frequency would shift if the lower dielectric EG mobile phase caused disruptions to the H-bonding environment of the
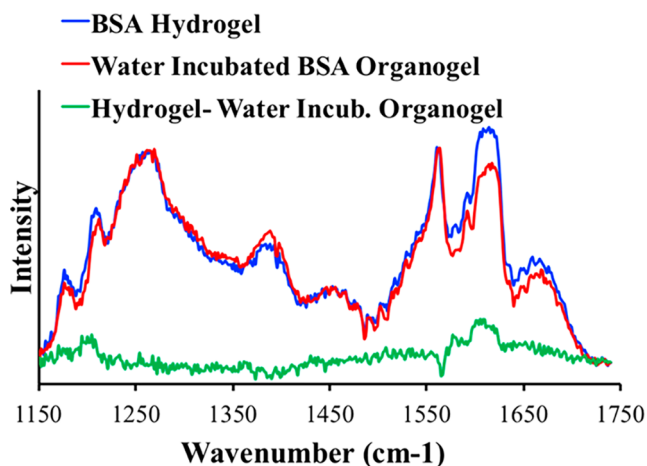
Figure 6. UVRR spectra of (blue) BSA hydrogel, (red) BSA organogel incubated in water, and (green) BSA hydrogel−water organogel incubated in water difference spectrum.

peptide backbone. AmI band frequency shifts in FT-IR spectra have been observed for HSA when bound water layers are stripped from the protein surface by the addition of EG.[80]

Water Content in BSA Organogels. NIR absorption spectroscopy was used to measure the water content in our BSA organogels to elucidate the microenvironment around the proteins of the organogel. Water strongly absorbs between 1900 and 1950 nm, whereas the EG has minimal absorption at these wavelengths.[81] The Supporting Information includes the

1400−2000 nm NIR absorbance of BSA organogels, the absorbance of EG−water mixtures, and the dependence of the 1915 nm absorbance as a function of water concentration. Details on the calculations of the water molar absorptivity at 1915 nm, the water concentration in bulk EG, and the calculation of the water concentration in our BSA organogels are also included in the Supporting Information.

The BSA organogels are in equilibrium with an EG mobile phase that contains ~0.08 M water. The 1400−2000 nm NIR absorbance spectra of the BSA organogel films are shown in Figure S5 in the Supporting Information. The strong absorption around 1900 nm stems from water that is partitioned into the organogel films. From these absorbance measurements, we calculate that the maximum BSA organogel water concentration is 8.0 ± 0.2 M.

To account for the small EG absorbance contributions to the total organogel absorbance, the absorbance of a 420 and 820 μm thick pure EG film was subtracted from the total BSA organogel absorbance. This subtraction overestimates the EG absorption since the EG content in the organogel is less than that of a pure EG film. The minimum BSA organogel water concentration is calculated using this EG subtracted absorbance. Our BSA organogels contain at least 6.5 ± 0.2 M water. We assume that the increased water content in the BSA organogels relative to the bulk EG mobile phase stems from solvation shell waters that are bound to the polymerized BSA proteins.

These BSA organogel water concentrations correspond to 1182−1475 water molecules per BSA protein. Small-angle neutron scattering experiments and theoretical calculations of a
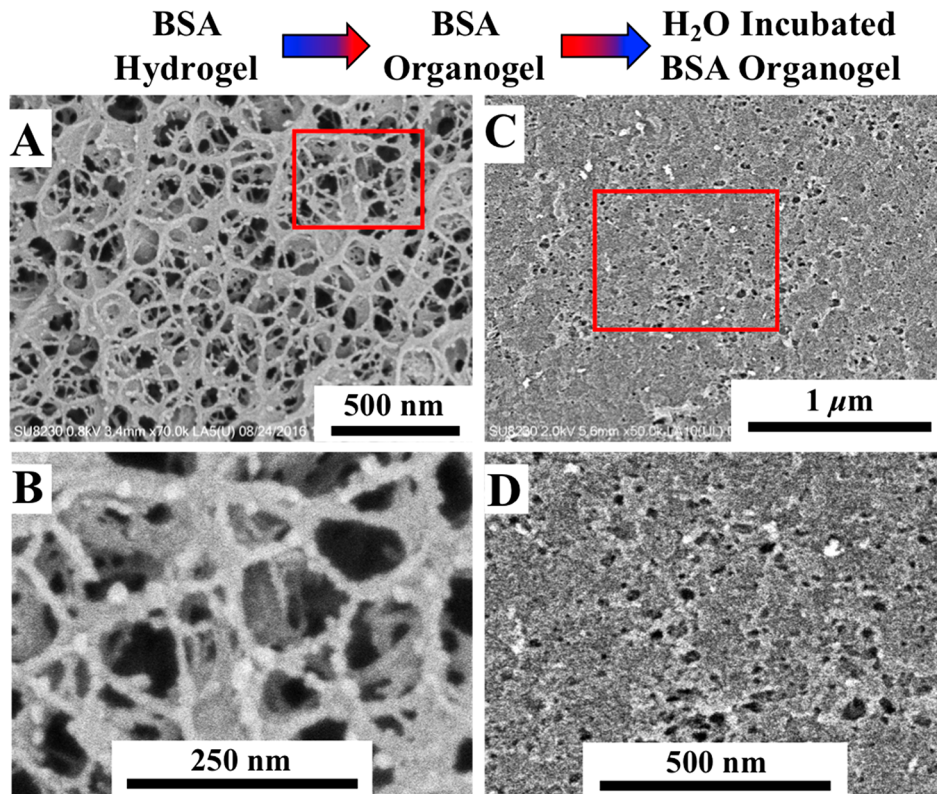

Figure 7. Cryo-SEM images comparing the morphology of BSA hydrogels (A, B) to that of the water incubated BSA organogels (C, D) after 40 min of sublimation and the application of a 2.5 nm Pt sputter coat. (A) BSA hydrogel; 70K magnification. (B) Enlarged area of BSA hydrogel, indicated by the red box in Figure 7A. (C) Water incubated BSA organogel; 50K magnification. (D) Enlarged area of water incubated BSA organogel, indicated by the red box in Figure 7C.

single water layer based on the BSA surface area have shown that the first solvation shell of BSA contains ~1070 water molecules.[63,82] Terahertz spectroscopy studies of albumin proteins in aqueous solutions found that the bound solvation shell waters, which have slower water relaxation times relative to bulk water, can extend ~0.85 nm[63] to ~1.5 nm[62] from the protein surface. Shiraga et al. estimated that the ~0.85 nm solvation shell contains ~3400 waters per BSA (3−4 hydration layers).[63]

The polymerized BSA proteins in pure EG retain more than one hydration layer. The 1182−1475 waters per BSA calculated in our BSA organogels correspond to 1.1−1.4 solvation shells. The retained BSA solvation shell waters most likely account for the constant UVRR AmI frequency measured in the BSA hydrogels and organogels.

This protein hydration layer is important for protein folding and the dynamics necessary for protein ligand binding and catalysis.[83−86] For example, it has been experimentally observed that there is a critical hydration level required for enzymatic activity (~a single monolayer of water).[63,83,86] Our pure protein organogel sensors and catalysts[39] retain much of their native protein activity in EG, at least in part, due to the retained hydration layers. A discussion on the retained protein hydration shell of BSA organogels is provided in the Supporting Information.

Water Incubated BSA Organogel Morphology. Only the water incubated BSA organogels could be investigated using Cryo-SEM. The BSA organogels could not be imaged because the EG mobile phase could not be sublimed from the BSA polymer structure. We hypothesize that the BSA organogel and water incubated BSA organogel morphologies are roughly similar. The irreversibility of the VPT indicates that the largest polymer morphology changes occur during the water to EG exchange. We believe that additional significant morphology changes during the solvent exchange back to water are unlikely.

The mobile phase exchange induces significant irreversible changes in the morphology of the BSA polymer network. As a result, there is an obvious difference between the BSA protein polymer network structure observed in Cryo-SEM images of the water incubated BSA organogel (Figure 7C,D) compared to that of the BSA hydrogel (Figure 7A,B). The water to EG exchange changes the BSA polymer morphology from an interconnected network of thin BSA polymer strands to a dense amorphous BSA polymer phase in the water incubated BSA organogel. This is accompanied by a decrease in the polymer pore diameters compared to that of the BSA hydrogel. The water incubated BSA organogel pore diameters range from ~5 to ~30 nm.

We could not resolve the individual BSA polymer strands in the dense amorphous BSA polymer phase. Thus, the topological properties of the organogel network, such as the number of interprotein cross-linked BSA in the protein polymer chains between polymer cross-links, cannot be estimated in the water incubated organogels, as we did for the BSA hydrogels. Thus, changes in the BSA polymer cross-link density cannot be determined from these Cryo-SEM images.

From titration studies, we found that these morphology changes are accompanied by a decrease in the BSA polymer surface area that is accessible to the mobile phase. The change in the mobile phase exposed BSA polymer surface area was examined by titrating the pH sensitive amino acid carboxyl

groups in the BSA hydrogels and in the water incubated organogels.

BSA contains 39 aspartic acid residues (pK_a 3.71) and 59 glutamic acid residues (pK_a 4.15).[61] The H^+ concentration required to titrate aqueous solutions containing BSA hydrogels or water incubated organogels from pH 6 to pH ~ 3.35 is directly proportional to the number of BSA carboxyl groups protonated. Only mobile phase accessible carboxyl groups on the BSA polymer surface are titratable. Carboxyl groups buried by the BSA polymer morphology change are not titrated because mobile phase diffusion to the buried polymer surface area is significantly slowed.

As shown in Figure 8, the water incubated BSA organogel titration curve is shifted to lower acid concentrations relative to
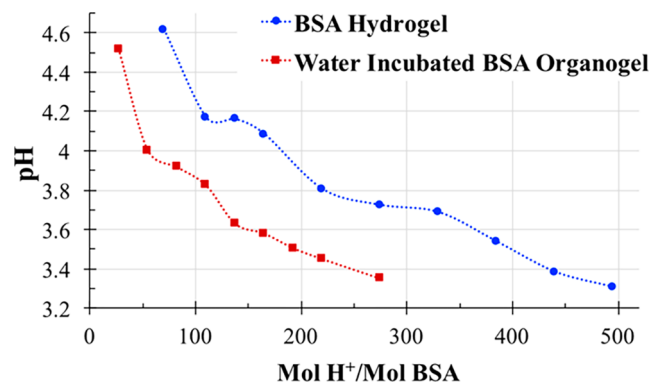

Figure 8. Titration curve of the BSA hydrogel before the water to EG exchange (blue), and the water incubated BSA organogel after the water to EG exchange and EG to water exchange (red). The titration is normalized to the number of moles of H^+ added to solution per mole of BSA in the sample.

that of the BSA hydrogel. The titration curves of the hydrogels and water incubated organogels can be directly compared because the titration is normalized to the number of moles of H^+ added per mole of BSA in the hydrogel or water incubated organogel.

The water incubated BSA organogels require ~2-fold less acid to protonate all titratable aspartic and glutamic acid residues compared to that of the BSA hydrogels. These titration results directly demonstrate that the VPT phase separation irreversibly changes the BSA polymer surface area exposed to the mobile phase. The VPT renders about half the polymer surface area inaccessible to the mobile phase.

It should also be noted that formation of amino acid side chain interactions may also occur during the phase separation and could contribute to the decrease in titratable carboxyl groups. Interactions between carboxylates and other amino acids may decrease the effective pK_a of those carboxylates. For example, salt bridges could form between the carboxylates and positively charged amino acids to stabilize the charged species.

Mechanism of Irreversible VPT Caused by EG Exchange. From these results, we are able to make certain conclusions on the mechanisms that actuate the VPT during the water to EG exchange. The large VPT that decreases the BSA organogel volume as a result of the EG exchange suggests that phase separation of the BSA polymer from the EG mobile phase occurs which induces a collapse of the polymer network. This BSA polymer phase separation is primarily driven by free energy of mixing changes, ΔG_{mix}.
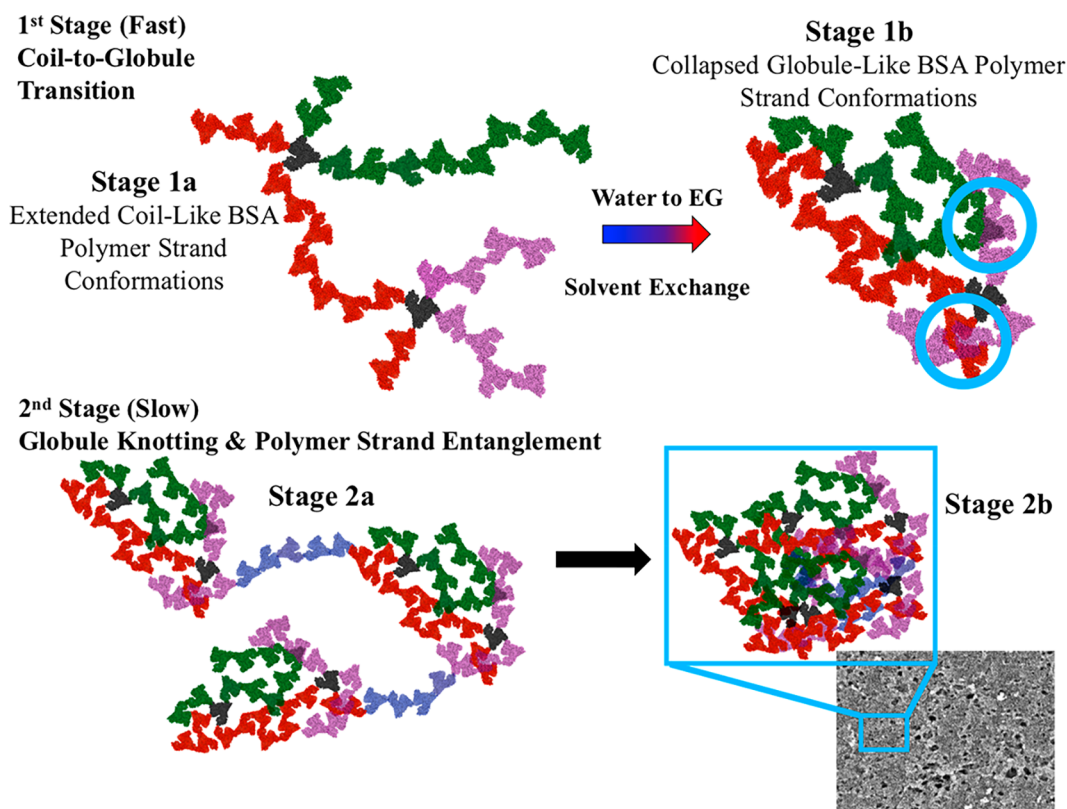
Figure 9. Illustration of the proposed kinetic two-stage phase separation of the BSA polymer that occurs during the water to EG exchange. The first stage (1a−1b) involves a fast coil-to-globule transition of the BSA polymer strands. This coil-to-globule transition decreases the distance between BSA polymer strands. Polymerized BSA on different protein polymer strands can form interprotein interactions where the BSA polymer strands are in close proximity, highlighted by the blue circles in stage 1b. These additional interprotein polymer strand interactions formed during phase separation increase the polymer cross-link density through physical polymer cross-linking, thus, preventing organogel reswelling. The second slower stage (2a−2b) of the phase separation involves knotting of the localized globules in the network and entanglement of the BSA polymer strands. This second stage further increases the BSA polymer density, resulting in the very dense BSA polymer phase observed in the water incubated organogel Cryo-SEM.

The UVRR experiments clearly demonstrate that the BSA secondary structure does not significantly change between the hydrogel and organogel. During fabrication of the BSA hydrogel, the proteins are immobilized by the glutaraldehyde cross-linking.[43] Protein immobilization stabilizes the native protein conformation, which inhibits protein denaturation by the introduced organic solvent mobile phase.[36] It is important to eliminate the possibility of protein structural changes because protein conformational changes could contribute to the VPT phenomenon,[25] particularly if the induced conformational change exposes amino acid side chains buried in the native protein core.

The BSA polymer VPT that occurs during the EG exchange is not caused by protein conformational changes but rather is induced by an unfavorable change in ΔG_{mix}, between the protein polymer and mobile phase as the concentration of EG increases. The hydrogel/organogel ΔG_{mix} is primarily determined by the Flory−Huggins polymer−solvent interaction parameter, χ.[23,65] Polymers in a good solvent are highly swollen and have small χ values because polymer−solvent interactions are favorable. In contrast, polymers in a poor solvent have larger χ values, and contain little solvent because polymer−polymer interactions are more favorable than polymer−mobile phase interactions.[87]

Flory theory predicts that when $\chi \geq 0.5$, phase separation of the polymer from the mobile phase will occur due to enthalpic

and/or entropic penalties resulting from the poor solvent interacting with the polymer chains.[23,87] It is extremely difficult to parse out which entropic or enthalpic contribution dominates this phase separation process because the hydrogel and subsequent organogel have a highly complex system of interactions between the protein polymer and mobile phase. The proteins have polypeptide chains made up of a specific sequence of 20 possible amino acid (AA) residues, that vary in their hydrophobic properties, charge state, and hydrogen bonding strength. This specific sequence of AA directs protein folding, leading to a protein conformation that exposes certain AA to the mobile phase and buries others in the core of the protein. Each AA in the protein will have different enthalpic and entropic contributions to the protein−mobile phase interactions depending on its chemical structure and depending on the neighboring amino acids.

The large swelling ratio of the BSA hydrogel in water indicates $\chi_{BSA-water} \ll 0.5$. The continuous decrease in BSA hydrogel volume that occurs upon EG exchange indicates that χ increases with increasing EG concentrations. When χ exceeds the critical value of 0.5, phase separation occurs. However, we cannot determine the EG concentration that initiates the phase separation from these existing data. A more careful investigation of the BSA hydrogel VPT generated with smaller incremental increases in the EG concentration is necessary. The critical EG concentration that induces phase separation

could be determined through titration of the BSA polymer carboxyl groups after equilibration in each EG/water solution. A large decrease in the solvent accessible polymer surface area would elucidate the EG concentration at which phase separation occurs.

This mobile phase exchange induced phase separation causes a collapse of the water swollen 3D protein polymer network. During phase separation, the polymer attempts to minimize its free energy, thus initiating conformational changes in the polymer strands that minimize its surface area in contact with the mobile phase.[88]

Polymer phase separation in a poor solvent is thought to occur as a (at least) two-stage process: a fast polymer strand collapse that induces a coil-to-globule-like transition in the polymer strands, followed by a slower stage that involves knotting of those globules and entanglement of the polymer strands.[89−91] We postulate that the BSA hydrogel to organogel transformation via the exchange from water to EG generates a similar kinetic two-stage phase separation, resulting in the dense amorphous BSA polymer phase observed in the water incubated organogel Cryo-SEM images, as illustrated in Figure 9.

The first stage of the phase separation involves a coil-to-globule transition of the BSA polymer strands (Figure 9, stage 1a−1b). The thin BSA polymer strands in the water swollen hydrogel have an extended coil-like conformation. These extended polymer strand conformations collapse into a globule-like conformation to minimize the polymer surface area in contact with the EG mobile phase. As depicted in Figure 9, stage 2a, this fast coil-to-globule transition creates localized high polymer density globules throughout the cross-linked network connected by stretched bridging BSA polymer strands.[90]

The coil-to-globule transition is followed by globule knotting, where these localized globules coalesce into a very high density BSA polymer phase.[89] Entanglement of the polymer strands within the dense BSA polymer phase also occurs in this second stage and increases over time.[92] This kinetic two-stage phase separation that occurs during the BSA hydrogel to organogel transformation results in the amorphous dense BSA polymer phase observed in the water incubated BSA organogel Cryo-SEM images (Figure 9, stage 2b).

The phase separation mechanisms of thermoresponsive polymers have extensively been studied, for linear poly(*N*-isopropylacrylamide),[87,93] polystyrene,[94] and poly(methyl methacrylate)[91] polymer chains in solution. The phase separation of cross-linked poly(*N*-isopropylacrylamide) hydrogel networks has also been investigate in polymer microparticles.[49] The rate of both stages of the phase separation is significantly slowed in a cross-linked polymer network due to the topological constraints compared to the linear polymer chains in solution.

The VPT induced by phase separation in synthetic organic polymers is typically reversible. Entanglement of the polymer strands slows globule swelling in a good solvent.[92] Hysteresis in the globule-to-coil transition of poly(*N*-isopropylacrylamide) polymers has been observed, where melting of the globule is slowed by physical entanglements formed in the globule state.[95]

In contrast, our BSA polymer system exhibits a completely irreversible VPT. Negligible polymer swelling was observed upon the exchange back to water for several weeks. We hypothesize that this irreversible VPT phenomenon of the pure protein polymer is caused by the formation of additional physical or chemical cross-links in the phase separated BSA polymer. The initial coil-to-globule transition and subsequent globule knotting decrease the distances between BSA polymer strands in the network. This allows formation of interprotein interactions between BSA proteins on different polymer strands that can act as polymer cross-links, indicated by the blue circles in Figure 9, stage 1b.

Additional interprotein strand interactions may include the formation of salt bridges or hydrogen bonds between AA side chains that act as physical polymer cross-links. Electrostatic and H-bonding interactions between AA side chains[100] are likely to form during the water to EG exchange because EG is less polar than water and is consequently a weaker H-bond acceptor/donor. Thus, the competitiveness of the solvent to H-bond with the AA side chains decreases when water is exchanged for EG such that the AA−AA interactions are enthalpically more favorable than AA−EG interactions. Chemical polymer cross-links could also form if dangling glutaraldehyde groups are present. Polymer strand entanglement could also create physical polymer cross-links in the BSA polymer network.

Thus, the elastic free energy of the BSA polymer network increases during the BSA hydrogel to organogel transition. The elastic free energy is an entropically derived restoring force that resists polymer strand conformational changes which are intrinsic to hydro-/organogel swelling or shrinking. Therefore, incubating the BSA organogel in water does not result in swelling due to a significant increase in the cross-link density of the BSA polymer network.

Finally, it must be noted that attempting to fabricate the BSA organogels using a single step solvent exchange where the BSA hydrogels are directly incubated in pure EG creates a material that is in a kinetically trapped state far from the thermodynamic equilibrium. The stepwise solvent exchange to EG allows the BSA polymer network to homogeneously shrink with increasing EG concentration prior to the phase separation event, that we believe occurs at higher EG concentrations. This creates a material much closer to the thermodynamic equilibrium state.

An interfacial skin layer can form in hydrogels when exposed to drastic changes in solvent quality that cause a phase separation induced VPT.[96] Skin layer formation has been utilized for drug release applications, where the drug is not released from the hydrogel material until the VPT of the skin layer is reversed.[97] However, formation of a skin layer in our photonic crystal organogel sensing materials may confound the sensor response. The BSA organogels fabricated using the stepwise solvent exchange swell in response to BSA−ligand binding.[39] In contrast, the single step solvent exchanged BSA organogels shrink in response to the ligand binding (unpublished data). The magnitude of these volume changes varies in the kinetically trapped BSA organogels depending on the time the BSA hydrogel was equilibrated in pure EG prior to ligand addition. This results in an unreliable sensor response for the single step solvent exchanged BSA organogels.

■ CONCLUSIONS

Using UVRR and IR spectroscopy, Cryo-SEM, and physical measurements of the gel volume and concentration of titratable amino acids, we characterized changes to the BSA secondary structure and BSA polymer morphology that accompanies the stepwise solvent exchange to EG. The mobile

phase exchange from water to EG transforms responsive BSA hydrogels into responsive BSA organogels. We determined the following:

(1) The BSA hydrogel is an interconnected network of thin BSA polymer strands with diameters roughly that of a single BSA protein. BSA hydrogel pores have diameters ranging from 50 to 200 nm. The molecular weight between polymer cross-links was approximated from the polymer strand lengths, which equal ~5−30 BSA or ~3 × 10^5 − 2 × 10^6 g/mol.

(2) The solvent exchange from the water mobile phase of the hydrogel to the EG mobile phase of the organogel causes a VPT that increases the BSA polymer volume fraction from $\phi_{hydrogel}$ = 6% to $\phi_{organogel}$ = 27%. The VPT is irreversible; $\phi_{water-incubated-organogel}$ = 27% after exchanging the EG mobile phase back to water.

(3) There is a ~4% increase in the population of α-helix secondary structure in the BSA organogel compared to that of the BSA hydrogel and native BSA monomers. These secondary structure changes are reversible; the UVRR AmIII$_3$ bands of water incubated BSA organogels are identical to those of the BSA hydrogels.

(4) The water incubated organogel UVRR spectrum does not contain contributions from EG, indicating that the EG mobile phase is qualitatively removed during exchange back to water.

(5) The NIR absorbance of water in the BSA organogels demonstrate that there is a higher water content in the BSA organogels compared to the bulk EG mobile phase. There are roughly 1200−1500 water molecules per BSA protein in the organogel, meaning 1.1−1.4 hydrations layers remain bound to the proteins.

(6) Irreversible BSA polymer morphology changes occur during EG exchange. The water incubated BSA organogel morphology drastically differs from that of the BSA hydrogel. The water incubated organogel morphology is a dense amorphous polymer phase with significantly smaller pore diameters (5−30 nm) compared to the BSA hydrogel pore diameters (50−200 nm).

(7) The hydrogel to organogel morphology change results in a decrease in the solvent exposed surface area. There are approximately 50% fewer titratable amino acid carboxyl groups in the BSA organogel than in the BSA hydrogel.

We determined that a phase separation of the BSA polymer and mobile phase causes the VPT that accompanies the hydrogel to organogel transformation. This phase separation is driven by free energy of mixing changes where the Flory−Huggins interaction parameter increases with increasing EG concentrations. This phase separation proceeds in two stages, a fast coil-to-globule transition followed by globule knotting and BSA polymer strand entanglement, that results in a dense amorphous BSA polymer morphology. Additional interprotein strand interactions that are formed in the phase separated BSA polymer state are the most likely source of the irreversible VPT phenomenon. Physical or chemical polymer cross-links increase the polymer cross-link density. Thus, the elastic free energy increases, resisting BSA polymer swelling when the mobile phase is exchanged back to water.

The irreversible VPT phenomena of our BSA polymer is advantageous for our photonic crystal sensing motif where BSA organogels sense BSA−ligand binding through an organogel swelling response. EG is a hydroscopic organic solvent and absorbs water vapor proportional to the relative humidity of the air. Water absorption by EG in the BSA organogel does not impact the sensor response because the addition of water will not reswell the organogel. This is in contrast to our previously fabricated evaporation resistant sensing materials that contain an ionic liquid mobile phase[16] which undergo a VPT in response to humidity changes.

ASSOCIATED CONTENT

Ⓢ Supporting Information

The Supporting Information is available free of charge at https://pubs.acs.org/doi/10.1021/acs.biomac.9b01522.

Cryo-SEM sample holder image, BSA solution and BSA hydrogel UVRR spectra, details on UVRR analysis, details of NIR absorbance experiments, including the 1400−2000 nm absorbance spectra of EG/water solutions and BSA organogels, calculations of BSA organogel water content, and a discussion on the retained hydration shell in BSA organogels (PDF)

AUTHOR INFORMATION

Corresponding Author
*E-mail: asher@pitt.edu.
ORCID Ⓘ
Natasha Lynn Smith: 0000-0001-9308-5178
Ryan S. Jakubek: 0000-0001-7880-9422
Sanford A. Asher: 0000-0003-1061-8747

Author Contributions

All authors have given approval to the final version of the manuscript.

Notes

The authors declare no competing financial interest.

ACKNOWLEDGMENTS

ABBREVIATIONS

VPT, volume phase transition; BSA, bovine serum albumin; EG, ethylene glycol; UVRR, UV resonance Raman; AA, amino acid

REFERENCES

(1) Elliott, J. E.; Macdonald, M.; Nie, J.; Bowman, C. N. Structure and Swelling of Poly (Acrylic Acid) Hydrogels: Effect of pH, Ionic Strength, and Dilution on the Crosslinked Polymer Structure. *Polymer* **2004**, *45*, 1503−1510.

(2) Lee, Y.-J.; Pruzinsky, S. A.; Braun, P. V. Glucose-Sensitive Inverse Opal Hydrogels: Analysis of Optical Diffraction Response. *Langmuir* **2004**, *20*, 3096−3106.

(3) Cai, Z.; Zhang, J.-T.; Xue, F.; Hong, Z.; Punihaole, D.; Asher, S. A. 2D Photonic Crystal Protein Hydrogel Coulometer for Sensing Serum Albumin Ligand Binding. *Anal. Chem.* **2014**, *86*, 4840−4847.

(4) Cai, Z.; Smith, N. L.; Zhang, J.-T.; Asher, S. A. Two-Dimensional Photonic Crystal Chemical and Biomolecular Sensors. *Anal. Chem.* **2015**, *87*, 5013−5025.

(5) Cai, Z.; Kwak, D. H.; Punihaole, D.; Hong, Z.; Velankar, S. S.; Liu, X.; Asher, S. A. A Photonic Crystal Protein Hydrogel Sensor for Candida albicans. *Angew. Chem., Int. Ed.* **2015**, *54*, 13036−13040.

(6) Lu, H. D.; Wheeldon, I. R.; Banta, S. Catalytic Biomaterials: Engineering Organophosphate Hydrolase to Form Self-Assembling Enzymatic Hydrogels. *Protein Eng., Des. Sel.* **2010**, *23*, 559−566.

(7) Kim, Y. H.; Campbell, E.; Yu, J.; Minteer, S. D.; Banta, S. Complete Oxidation of Methanol in Biobattery Devices Using a Hydrogel Created from Three Modified Dehydrogenases. *Angew. Chem., Int. Ed.* **2013**, *52*, 1437−1440.

(8) Hoffman, A. S. Hydrogels for Biomedical Applications. *Adv. Drug Delivery Rev.* **2012**, *64*, 18−23.

(9) Baler, K.; Michael, R.; Szleifer, I.; Ameer, G. A. Albumin Hydrogels Formed by Electrostatically Triggered Self-Assembly and Their Drug Delivery Capability. *Biomacromolecules* **2014**, *15*, 3625−3633.

(10) Leach, J. B.; Schmidt, C. E. Characterization of Protein Release from Photocrosslinkable Hyaluronic Acid-Polyethylene Glycol Hydrogel Tissue Engineering Scaffolds. *Biomaterials* **2005**, *26*, 125−135.

(11) Kamoun, E. A.; Kenawy, E.-R. S.; Chen, X. A Review on Polymeric Hydrogel Membranes for Wound Dressing Applications: PVA-Based Hydrogel Dressings. *J. Adv. Res.* **2017**, *8*, 217−233.

(12) Idris, A.; Man, Z.; Maulud, A.; Khan, M. Effects of Phase Separation Behavior on Morphology and Performance of Polycarbonate Membranes. *Membranes* **2017**, *7*, 21−39.

(13) Gerlach, G., Arndt, K.-F., Eds. *Hydrogel Sensors and Actuators: Engineering and Technology*; Springer Series on Chemical Sensors and Biosensors Vol. 6; Springer-Verlag Berlin Heidelberg: Dresden, 2010.

(14) Asher, S. A.; Holtz, J.; Liu, L.; Wu, Z. Self-Assembly Motif for Creating Submicron Periodic Materials. Polymerized Crystalline Colloidal Arrays. *J. Am. Chem. Soc.* **1994**, *116*, 4997−4998.

(15) Zhang, J.-T.; Wang, L.; Luo, J.; Tikhonov, A.; Kornienko, N.; Asher, S. A. 2-D Array Photonic Crystal Sensing Motif. *J. Am. Chem. Soc.* **2011**, *133*, 9152−9155.

(16) Smith, N. L.; Hong, Z.; Asher, S. A. Responsive Ionic Liquid-Polymer 2D Photonic Crystal Gas Sensors. *Analyst (Cambridge, U. K.)* **2014**, *139*, 6379−6386.

(17) Walker, J.; Kimble, K.; Asher, S. Photonic Crystal Sensor for Organophosphate Nerve Agents Utilizing the Organophosphorus Hydrolase Enzyme. *Anal. Bioanal. Chem.* **2007**, *389*, 2115−2124.

(18) Walker, J. P.; Asher, S. A. Acetylcholinesterase-Based Organophosphate Nerve Agent Sensing Photonic Crystal. *Anal. Chem.* **2005**, *77*, 1596−1600.

(19) Kamenjicki, M.; Lednev, I. K.; Asher, S. A. Photoresponsive Azobenzene Photonic Crystals. *J. Phys. Chem. B* **2004**, *108*, 12637−12639.

(20) Sharma, A. C.; Jana, T.; Kesavamoorthy, R.; Shi, L.; Virji, M. A.; Finegold, D. N.; Asher, S. A. A General Photonic Crystal Sensing Motif: Creatinine in Bodily Fluids. *J. Am. Chem. Soc.* **2004**, *126*, 2971−2977.

(21) Goponenko, A. V.; Asher, S. A. Modeling of Stimulated Hydrogel Volume Changes in Photonic Crystal Pb2+ Sensing Materials. *J. Am. Chem. Soc.* **2005**, *127*, 10753−10759.

(22) Wu, C.; Zhou, S. Volume Phase Transition of Swollen Gels: Discontinuous or Continuous? *Macromolecules* **1997**, *30*, 574−576.

(23) Flory, P. J. *Principles of Polymer Chemistry*; Cornell University Press: Ithaca, NY, 1953.

(24) Hirotsu, S.; Hirokawa, Y.; Tanaka, T. Volume-Phase Transitions of Ionized N-Isopropylacrylamide Gels. *J. Chem. Phys.* **1987**, *87*, 1392−1395.

(25) Cai, Z.; Luck, L. A.; Punihaole, D.; Madura, J. D.; Asher, S. A. Photonic Crystal Protein Hydrogel Sensor Materials Enabled by Conformationally Induced Volume Phase Transition. *Chem. Sci.* **2016**, *7*, 4557−4562.

(26) Gao, X.; Lyu, S.; Li, H. Decorating a Blank Slate Protein Hydrogel: A General and Robust Approach for Functionalizing Protein Hydrogels. *Biomacromolecules* **2017**, *18*, 3726−3732.

(27) Xu, X.; Xu, Z.; Yang, X.; He, Y.; Lin, R. Construction and Characterization of a Pure Protein Hydrogel for Drug Delivery Application. *Int. J. Biol. Macromol.* **2017**, *95*, 294−298.

(28) Heck, T.; Faccio, G.; Richter, M.; Thöny-Meyer, L. Enzyme-Catalyzed Protein Crosslinking. *Appl. Microbiol. Biotechnol.* **2013**, *97*, 461−475.

(29) de Vries, A.; Hendriks, J.; van der Linden, E.; Scholten, E. Protein Oleogels from Protein Hydrogels via a Stepwise Solvent Exchange Route. *Langmuir* **2015**, *31*, 13850−13859.

(30) Scholten, E. Protein Oleogels: Network Formation of Proteins in Hydrophobic Conditions. In *Edible Oleogels*, 2nd ed.; Marangoni, A. G., Garti, N., Eds.; AOCS Press, 2018; Chapter 12, pp 285−305.

(31) Fjerbaek, L.; Christensen, K. V.; Norddahl, B. A Review of the Current State of Biodiesel Production using Enzymatic Transesterification. *Biotechnol. Bioeng.* **2009**, *102*, 1298−1315.

(32) Carrea, G.; Riva, S. Properties and Synthetic Applications of Enzymes in Organic Solvents. *Angew. Chem., Int. Ed.* **2000**, *39*, 2226−2254.

(33) Jacquet, P.; Daudé, D.; Bzdrenga, J.; Masson, P.; Elias, M.; Chabrière, E. Current and Emerging Strategies for Organophosphate Decontamination: Special Focus on Hyperstable Enzymes. *Environ. Sci. Pollut. Res.* **2016**, *23*, 8200−8218.

(34) Yang, F.; Wild, J. R.; Russell, A. J. Nonaqueous Biocatalytic Degradation of a Nerve Gas Mimic. *Biotechnol. Prog.* **1995**, *11*, 471−474.

(35) Mattos, C.; Ringe, D. Proteins in Organic Solvents. *Curr. Opin. Struct. Biol.* **2001**, *11*, 761−764.

(36) Stepankova, V.; Bidmanova, S.; Koudelakova, T.; Prokop, Z.; Chaloupkova, R.; Damborsky, J. Strategies for Stabilization of Enzymes in Organic Solvents. *ACS Catal.* **2013**, *3*, 2823−2836.

(37) Iyer, P. V.; Ananthanarayan, L. Enzyme Stability and Stabilization—Aqueous and Non-Aqueous Environment. *Process Biochem. (Oxford, U. K.)* **2008**, *43*, 1019−1032.

(38) Zdarta, J.; Meyer, A.; Jesionowski, T.; Pinelo, M. A General Overview of Support Materials for Enzyme Immobilization: Characteristics, Properties, Practical Utility. *Catalysts* **2018**, *8*, 92−119.

(39) Smith, N. L.; Coukouma, A. E.; Wilson, D. C.; Ho, B.; Gray, V. P.; Asher, S. A. Stimuli Responsive Pure Protein Organogel Sensors and Biocatalytic Materials. *ACS Appl. Mater. Interfaces* **2019**, in press; DOI: 10.1021/acsami.9b18191.

(40) Cui, J. D.; Jia, S. R. Optimization Protocols and Improved Strategies of Cross-linked Enzyme Aggregates Technology: Current Development and Future Challenges. *Crit. Rev. Biotechnol.* **2015**, *35*, 15−28.

(41) López-Gallego, F.; Betancor, L.; Mateo, C.; Hidalgo, A.; Alonso-Morales, N.; Dellamora-Ortiz, G.; Guisán, J. M.; Fernández-Lafuente, R. Enzyme Stabilization by Glutaraldehyde Crosslinking of Adsorbed Proteins on Aminated Supports. *J. Biotechnol.* **2005**, *119*, 70−75.

(42) Kartal, F.; Janssen, M. H. A.; Hollmann, F.; Sheldon, R. A.; Kılınc, A. Improved Esterification Activity of Candida Rugosa Lipase in Organic Solvent by Immobilization as Cross-linked Enzyme Aggregates (CLEAs). *J. Mol. Catal. B: Enzym.* **2011**, *71*, 85−89.

(43) Sheldon, R. A.; Schoevaart, R.; Van Langen, L. M. Cross-linked Enzyme Aggregates (CLEAs): A Novel and Versatile Method for Enzyme Immobilization (a review). *Biocatal. Biotransform.* **2005**, *23*, 141−147.

(44) Homaei, A. A.; Sariri, R.; Vianello, F.; Stevanato, R. Enzyme Immobilization: An Update. *J. Chem. Biol.* **2013**, *6*, 185−205.

(45) Curry, S.; Brick, P.; Franks, N. P. Fatty Acid Binding to Human Serum Albumin: New Insights from Crystallographic Studies. *Biochim. Biophys. Acta, Mol. Cell Biol. Lipids* **1999**, *1441*, 131−140.

(46) Evoli, S.; Mobley, D. L.; Guzzi, R.; Rizzuti, B. Multiple Binding Modes of Ibuprofen in Human Serum Albumin Identified by Absolute

Binding Free Energy Calculations. *Phys. Chem. Chem. Phys.* **2016**, *18*, 32358−32368.

(47) Mikhonin, A. V.; Bykov, S. V.; Myshakina, N. S.; Asher, S. A. Peptide Secondary Structure Folding Reaction Coordinate: Correlation between UV Raman Amide III Frequency, Ψ Ramachandran Angle, and Hydrogen Bonding. *J. Phys. Chem. B* **2006**, *110*, 1928−1943.

(48) Wu, T.-Y.; Zrimsek, A. B.; Bykov, S. V.; Jakubek, R. S.; Asher, S. A. Hydrophobic Collapse Initiates the Poly(N-isopropylacrylamide) Volume Phase Transition Reaction Coordinate. *J. Phys. Chem. B* **2018**, *122*, 3008−3014.

(49) Wu, C. A Comparison Between the 'Coil-to-Globule' Transition of Linear Chains and the 'Volume Phase Transition' of Spherical Microgels. *Polymer* **1998**, *39*, 4609−4619.

(50) Erickson, H. P. Size and Shape of Protein Molecules at the Nanometer Level Determined by Sedimentation, Gel Filtration, and Electron Microscopy. *Biol. Proced. Online* **2009**, *11*, 32−51.

(51) Bykov, S.; Lednev, I.; Ianoul, A.; Mikhonin, A.; Munro, C.; Asher, S. A. Steady-State and Transient Ultraviolet Resonance Raman Spectrometer for the 193−270 nm Spectral Region. *Appl. Spectrosc.* **2005**, *59*, 1541−1552.

(52) Heuser, J. E. The Origins and Evolution of Freeze-Etch Electron Microscopy. *Microscopy* **2011**, *60*, S3−S29.

(53) Schneider, C. A.; Rasband, W. S.; Eliceiri, K. W. NIH Image to ImageJ: 25 years of Image Analysis. *Nat. Methods* **2012**, *9*, 671.

(54) Migneault, I.; Dartiguenave, C.; Bertrand, M. J.; Waldron, K. C. Glutaraldehyde: Behavior in Aqueous Solution, Reaction with Proteins, and Application to Enzyme Crosslinking. *BioTechniques* **2004**, *37*, 790−802.

(55) Huang, B. X.; Kim, H.-Y.; Dass, C. Probing Three-Dimensional Structure of Bovine Serum Albumin by Chemical Cross-linking and Mass Spectrometry. *J. Am. Soc. Mass Spectrom.* **2004**, *15* (8), 1237−1247.

(56) Apkarian, R. P.; Wright, E. R.; Seredyuk, V. A.; Eustis, S.; Lyon, L. A.; Conticello, V. P.; Menger, F. M. In-Lens Cryo-High Resolution Scanning Electron Microscopy: Methodologies for Molecular Imaging of Self-Assembled Organic Hydrogels. *Microsc. Microanal.* **2003**, *9*, 286−295.

(57) Wright, E. R.; Conticello, V. P.; Apkarian, R. P. Morphological Characterization of Elastin-Mimetic Block Copolymers Utilizing Cryo- and Cryoetch-HRSEM. *Microsc. Microanal.* **2003**, *9*, 171−182.

(58) Vezie, D. L.; Thomas, E. L.; Adams, W. W. Low-Voltage, High-Resolution Scanning Electron Microscopy: A New Characterization Technique for Polymer Morphology. *Polymer* **1995**, *36*, 1761−1779.

(59) Guo, Q. *Polymer Morphology: Principles, Characterization, and Processing*; John Wiley & Sons, Incorporated: New York, 2016.

(60) Lou, X.; Munro, S.; Wang, S. Drug Release Characteristics of Phase Separation pHEMA Sponge Materials. *Biomaterials* **2004**, *25*, 5071−5080.

(61) Majorek, K. A.; Porebski, P. J.; Dayal, A.; Zimmerman, M. D.; Jablonska, K.; Stewart, A. J.; Chruszcz, M.; Minor, W. Structural and Immunologic Characterization of Bovine, Horse, and Rabbit Serum Albumins. *Mol. Immunol.* **2012**, *52*, 174−182.

(62) Bye, J. W.; Meliga, S.; Ferachou, D.; Cinque, G.; Zeitler, J. A.; Falconer, R. J. Analysis of the Hydration Water around Bovine Serum Albumin Using Terahertz Coherent Synchrotron Radiation. *J. Phys. Chem. A* **2014**, *118*, 83−88.

(63) Shiraga, K.; Ogawa, Y.; Kondo, N. Hydrogen Bond Network of Water around Protein Investigated with Terahertz and Infrared Spectroscopy. *Biophys. J.* **2016**, *111*, 2629−2641.

(64) Gu, Y.; Zhao, J.; Johnson, J. A. A (Macro)Molecular-Level Understanding of Polymer Network Topology. *Trends Chem.* **2019**, *1*, 318−334.

(65) White, E. M.; Yatvin, J.; Grubbs, J. B., III; Bilbrey, J. A.; Locklin, J. Advances in Smart Materials: Stimuli-Responsive Hydrogel Thin Films. *J. Polym. Sci., Part B: Polym. Phys.* **2013**, *51*, 1084−1099.

(66) Marmorat, C.; Arinstein, A.; Koifman, N.; Talmon, Y.; Zussman, E.; Rafailovich, M. Cryo-Imaging of Hydrogels Supermolecular Structure. *Sci. Rep.* **2016**, *6*, 25495.

(67) Murayama, K.; Tomida, M. Heat-Induced Secondary Structure and Conformation Change of Bovine Serum Albumin Investigated by Fourier Transform Infrared Spectroscopy. *Biochemistry* **2004**, *43*, 11526−11532.

(68) Tanaka, T.; Fillmore, D.; Sun, S.-T.; Nishio, I.; Swislow, G.; Shah, A. Phase Transitions in Ionic Gels. *Phys. Rev. Lett.* **1980**, *45*, 1636−1639.

(69) Punihaole, D.; Jakubek, R. S.; Workman, R. J.; Asher, S. A. Interaction Enthalpy of Side Chain and Backbone Amides in Polyglutamine Solution Monomers and Fibrils. *J. Phys. Chem. Lett.* **2018**, *9*, 1944−1950.

(70) Wang, Y.; Purrello, R.; Georgiou, S.; Spiro, T. G. UVRR Spectroscopy of the Peptide Bond. 2. Carbonyl H-Bond Effects on the Ground- and Excited-State Structures of N-Methylacetamide. *J. Am. Chem. Soc.* **1991**, *113*, 6368−6377.

(71) Jakubek, R. S.; White, S. E.; Asher, S. A. UV Resonance Raman Structural Characterization of an (In)soluble Polyglutamine Peptide. *J. Phys. Chem. B* **2019**, *123*, 1749−1763.

(72) Punihaole, D.; Jakubek, R. S.; Dahlburg, E. M.; Hong, Z.; Myshakina, N. S.; Geib, S.; Asher, S. A. UV Resonance Raman Investigation of the Aqueous Solvation Dependence of Primary Amide Vibrations. *J. Phys. Chem. B* **2015**, *119*, 3931−3939.

(73) Jakubek, R. S.; Workman, R. J.; White, S. E.; Asher, S. A. Polyglutamine Solution-State Structural Propensity Is Repeat Length Dependent. *J. Phys. Chem. B* **2019**, *123*, 4193−4203.

(74) Asher, S. A.; Ianoul, A.; Mix, G.; Boyden, M. N.; Karnoup, A.; Diem, M.; Schweitzer-Stenner, R. Dihedral ψ Angle Dependence of the Amide III Vibration: A Uniquely Sensitive UV Resonance Raman Secondary Structural Probe. *J. Am. Chem. Soc.* **2001**, *123*, 11775−11781.

(75) Jakubek, R. S.; Handen, J.; White, S. E.; Asher, S. A.; Lednev, I. K. Ultraviolet Resonance Raman Spectroscopic Markers for Protein Structure and Dynamics. *TrAC, Trends Anal. Chem.* **2018**, *103*, 223−229.

(76) Oladepo, S. A.; Xiong, K.; Hong, Z.; Asher, S. A.; Handen, J.; Lednev, I. K. UV Resonance Raman Investigations of Peptide and Protein Structure and Dynamics. *Chem. Rev.* **2012**, *112*, 2604−2628.

(77) Takeda, K.; Shigeta, M.; Aoki, K. Secondary Structures of Bovine Serum Albumin in Anionic and Cationic Surfactant Solutions. *J. Colloid Interface Sci.* **1987**, *117*, 120−126.

(78) Moriyama, Y.; Watanabe, E.; Kobayashi, K.; Harano, H.; Inui, E.; Takeda, K. Secondary Structural Change of Bovine Serum Albumin in Thermal Denaturation up to 130 °C and Protective Effect of Sodium Dodecyl Sulfate on the Change. *J. Phys. Chem. B* **2008**, *112*, 16585−16589.

(79) Wasacz, F. M.; Olinger, J. M.; Jakobsen, R. J. Fourier Transform Infrared Studies of Proteins using Nonaqueous Solvents. Effects of Methanol and Ethylene Glycol on Albumin and Immunoglobulin G. *Biochemistry* **1987**, *26*, 1464−1470.

(80) Jakobsen, R. J.; Wasacz, F. M.; Brasch, J. W.; Smith, K. B. The Relationship of Bound Water to the IR Amide I Bandwidth of Albumin. *Biopolymers* **1986**, *25*, 639−654.

(81) GuidedWave, An Introduction to Online NIR Water Measurements in Liquid Samples. AZO Mater. [Online], Jan. 25, 2019. https://www.azom.com/article.aspx?ArticleID=17511 (accessed May 27, 2019).

(82) Rejou-Michel, A.; Henry, F.; Villardi, M. d.; Delmotte, M. Protein and Ion Hydration Variation in Fixed Aqueous Solutions: Measurement by Dielectric Decrement. *Phys. Med. Biol.* **1985**, *30*, 831−837.

(83) Rupley, J. A.; Careri, G. Protein Hydration and Function. In *Advances in Protein Chemistry*; Anfinsen, C. B., Richards, F. M., Edsall, J. T., Eisenberg, D. S., Eds.; Academic Press, 1991; Vol. *41*, pp 37−172.

(84) Schmitke, J. L.; Wescott, C. R.; Klibanov, A. M. The Mechanistic Dissection of the Plunge in Enzymatic Activity upon Transition from Water to Anhydrous Solvents. *J. Am. Chem. Soc.* **1996**, *118*, 3360−3365.

(85) Laage, D.; Elsaesser, T.; Hynes, J. T. Water Dynamics in the Hydration Shells of Biomolecules. *Chem. Rev.* **2017**, *117*, 10694−10725.

(86) Brovchenko, I.; Oleinikova, A. Which Properties of a Spanning Network of Hydration Water Enable Biological Functions? *ChemPhysChem* **2008**, *9*, 2695−2702.

(87) Wang, R.; Wang, Z.-G. Theory of Polymer Chains in Poor Solvent: Single-Chain Structure, Solution Thermodynamics, and Θ Point. *Macromolecules* **2014**, *47*, 4094−4102.

(88) Raos, G.; Allegra, G. Chain Collapse and Phase Separation in Poor-Solvent Polymer Solutions: A Unified Molecular Description. *J. Chem. Phys.* **1996**, *104*, 1626−1645.

(89) Grosberg, A. Y.; Kuznetsov, D. V. Single-Chain Collapse or Precipitation? Kinetic Diagram of the States of a Polymer Solution. *Macromolecules* **1993**, *26*, 4249−4251.

(90) Halperin, A.; Goldbart, P. M. Early Stages of Homopolymer Collapse. *Phys. Rev. E: Stat. Phys., Plasmas, Fluids, Relat. Interdiscip. Top.* **2000**, *61*, 565−573.

(91) Maki, Y. Chain Collapse and Aggregation in Dilute Solutions of Poly(Methyl-Methacrylate) Below the Theta Temperature. *Polym. J. (Tokyo, Jpn.)* **2014**, *46*, 641.

(92) Lee, N.-K.; Abrams, C. F.; Johner, A.; Obukhov, S. Arrested Swelling of Highly Entangled Polymer Globules. *Phys. Rev. Lett.* **2003**, *90*, 225504.

(93) Wang, X.; Qiu, X.; Wu, C. Comparison of the Coil-to-Globule and the Globule-to-Coil Transitions of a Single Poly(N-isopropylacrylamide) Homopolymer Chain in Water. *Macromolecules* **1998**, *31*, 2972−2976.

(94) Chu, B.; Ying, Q.; Grosberg, A. Y. Two-Stage Kinetics of Single-Chain Collapse. Polystyrene in Cyclohexane. *Macromolecules* **1995**, *28*, 180−189.

(95) Wu, C.; Wang, X. Globule-to-Coil Transition of a Single Homopolymer Chain in Solution. *Phys. Rev. Lett.* **1998**, *80*, 4092−4094.

(96) Matsuo, E. S.; Tanaka, T. Patterns in Shrinking Gels. *Nature* **1992**, *358*, 482−485.

(97) Yoshida, R.; Sakai, K.; Okano, T.; Sakurai, Y. Surface-Modulated Skin Layers of Thermal Responsive Hydrogels as On-Off Switches: II. Drug Permeation. *J. Biomater. Sci., Polym. Ed.* **1992**, *3*, 243−252.

(98) Xing, R.; Yuan, C.; Li, S.; Song, J.; Li, J.; Yan, X. Charge-Induced Secondary Structure Transformation of Amyloid-Derived Dipeptide Assemblies from β-Sheet to α-Helix. *Angew. Chem., Int. Ed.* **2018**, *57*, 1537−1542.

(99) Yuan, T.; Xu, Y.; Fei, J.; Xue, H.; Li, X.; Wang, C.; Fytas, G.; Li, J. The Ultrafast Assembly of a Dipeptide Supramolecular Organogel and its Phase Transition from Gel to Crystal. *Angew. Chem., Int. Ed.* **2019**, *58*, 11072−11077.

(100) Yuan, C.; Ji, W.; Xing, R.; Li, J.; Gazit, E.; Yan, X. Hierarchically oriented organization in supramolecular peptide crystals. *Nat. Rev. Chem.* **2019**, *3*, 567−588.